AUTHOR(S):

Yamaguchi, Tatsuma; Matsuzaki, Yuichiro; Saijo, Soya; Watanabe, Hideyuki; Mizuochi, Norikazu; Ishi-Hayase, Junko

RAPID COMMUNICATION

Check for updates

Control of all the transitions between ground state manifolds of nitrogen vacancy centers in diamonds by applying external magnetic driving fields

Tatsuma Yamaguchi[1], Yuichiro Matsuzaki[2] , Soya Saijo[1], Hideyuki Watanabe[2], Norikazu Mizuochi[3] , and Junko Ishi-Hayase[1,4*]

[1]School of Fundamental Science and Technology, Keio University, 3-14-1 Hiyoshi, Kohoku-ku, Yokohama 223-8522, Japan
[2]Device Technology Research Institute, National institute of Advanced Industrial Science and Technology (AIST), Central2, 1-1-1 Umezono, Tsukuba, Ibaraki 305-8568, Japan
[3]Institute for Chemical Research, Kyoto University, Gokasho, Uji, Kyoto 611-0011, Japan
[4]Center for Spintronics Research Network, Keio University, 3-14-1 Hiyoshi, Kohoku-ku, Yokohama 223-8522, Japan

*E-mail: hayase@appi.keio.ac.jp

We demonstrate control of all the three transitions among the ground state sublevels of NV centers by applying magnetic driving fields. To address the states of a specific NV axis among the four axes, we apply a magnetic field orthogonal to the NV axis. We control two transitions by microwave pulses and the remaining transition by radio frequency (RF) pulses. In particular, we investigate the dependence of Rabi oscillations on the frequency and intensity of the RF pulses. In addition, we perform a π pulse by the RF pulses and measured the coherence time between the ground state sublevels. Our results pave the way for control of NV centers for the realization of quantum information processing and quantum sensing. © 2020 The Japan Society of Applied Physics

Supplementary material for this article is available online

Nitrogen-vacancy (NV) centers in diamonds is a promising system for the realization of quantum technology that includes quantum information processing, quantum communications, and quantum sensing. The established controllability[1,2] and long coherence time[3–5] shall be prerequisites for quantum computation. The coherent coupling between NV centers and optical photons serves as a method of realizing quantum communication.[6–10] The spin–spin coupling in diamonds has the potential to realize a quantum simulator as proposed in Ref. 11. Moreover, owing to the high spatial resolution and high sensitivity at room temperature and atmospheric pressure, one of the most practical applications of NV centers is quantum sensing.[12–14] Magnetic fields,[13–16] electric fields,[17–22] and temperatures[23–31] have been measured through NV centers in diamonds.

An NV center in a diamond is a spin-1 system, and there are three states in the ground state manifolds. However, only two of these states are typically controlled, and the remaining state is not addressed using frequency selectivity. Recently, new schemes have been proposed to use all three states in the ground state manifolds; they have demonstrated high-sensitivity magnetic field sensing,[32] high-sensitivity temperature sensing,[24] and AC magnetic field sensing that does not require pulse control.[33,34] Moreover, the three levels of the NV centers can be used for a quantum memory of superconducting qubits where a bright state and a dark state of the NV centers are used.[35–37] Further developments are expected using the Δ-system.[38,39]

To exploit the full potential of the spin 1 system, it is important to control all three transitions among the ground state sublevels of the NV centers. Such full control of the three transitions has been investigated by using a combination of magnetic fields,[40] lasers,[41,42] mechanical vibrations,[43–45] and electric fields.[46] In the existing approach, a complicated fabrication in diamond is required to realize such full control of the three transitions at room

temperature because such a scheme requires either mechanical vibrations of the diamond[43–45,47] or an application of electric fields.[46]

In this study, we demonstrate a simple control of the three transitions among the ground state sublevels of the NV centers using driving magnetic fields at room temperature. Importantly, our scheme does not require a special fabrication of the diamond substrate, unlike in the case of the existing scheme,[43,44] which can provide a practical advantage. We implement Rabi oscillations of two transitions using microwave pulses, whereas we drive the remaining transition using radio frequency (RF) pulses. We sweep the pulse duration and detect the state of the spin using optical measurements. In particular, we investigate the dependence of Rabi oscillations on the frequency and intensity of the RF pulses. Further, we compare the experimental results with the theoretical results and observe good agreement between them.

Figure 1(a) details the energy levels of NV centers without an external DC magnetic field. The spin 1 system has three states: $|0\rangle$, $|B\rangle = \frac{1}{\sqrt{2}}(|1\rangle + |-1\rangle)$, and $|D\rangle = \frac{1}{\sqrt{2}}(|1\rangle - |-1\rangle)$. NV centers have four possible crystallographic axes, and their levels are degenerate under zero magnetic field. To address the states of a specific NV axis, we apply a magnetic field orthogonal to one of the NV axes so that the resonant frequencies of the NV centers with the other three axes become far-detuned. The orthogonal magnetic field lifts the degeneracy as illustrated in Fig. 1(b), and we obtain $|B\rangle$, $|D\rangle$, and $|0\rangle$ as the energy eigenstates of the Hamiltonian. Importantly, AC magnetic fields can induce all the transitions between these three states, as we will describe later. This is a stark contrast with the case when $|1\rangle$, $|-1\rangle$, and $|0\rangle$ are the energy eigenstates when the applied magnetic field is parallel to the NV axis, which was typically adopted in the previous experiments where we cannot induce the transition between $|1\rangle$ and $|-1\rangle$ by applying AC magnetic fields.

We describe the theory about how all transitions between ground state manifolds of NV centers can be controlled by

© 2020 The Japan Society of Applied Physics
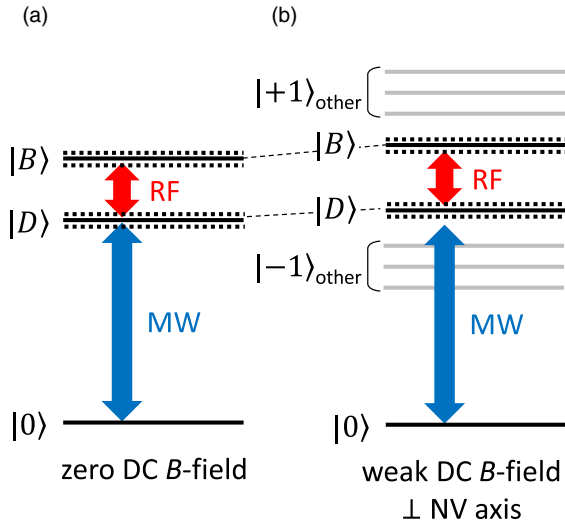
Fig. 1. (Color online) Energy levels of NV centers (a) without/(b)with an applied DC magnetic field perpendicular to one of the four possible crystallographic axes. Under the DC magnetic field, we focus on the NV centers with axes perpendicular to the applied DC magnetic field by frequency selectivity. Orthogonal magnetic fields change the effective strain so that the energy splitting between the bright state and dark state becomes larger. When resonant RF field is applied, Aulter–Towns (AT) splitting occurs and there are four states (dotted lines). The original data is presented in Ref. 34.

applying AC magnetic fields. Since we explain the details of the theory in the supplementary file, which is available online at stacks.iop.org/JJAP/59/110907/mmedia, we explain an outline of the derivation in the main text. Here, let us consider a case to apply a DC magnetic field orthogonal to the NV axis. The Hamiltonian of the NV center with the magnetic field orthogonal to the NV axis[34] is described as

$$
\begin{aligned}
H_{NV} =\ & D\hat{S}_z^2 + E_x(\hat{S}_x^2 - \hat{S}_y^2) \\
& + E_y(\hat{S}_x\hat{S}_y + \hat{S}_y\hat{S}_x) + g\mu_b B_x\hat{S}_x,
\end{aligned}
\tag{1}
$$

where $\hat{S}$ is the spin-1 operator of the electronic spin; D is the zero-field splitting; E_x and E_y are the strains along the x and y directions, respectively; $g\mu_b B_x$ is the Zeeman splitting. The *x-direction* of the NV center is defined as the direction of the applied magnetic field, without loss of generality. Under the condition $D \gg g\mu_b B_x \gg E_y$, we can simplify the Hamiltonian as follows

$$
H_{NV} \simeq D'\hat{S}_z^2 + E_x'(\hat{S}_x^2 - \hat{S}_y^2),
\tag{2}
$$

$$
D' = D + \frac{3}{2}\frac{(g\mu_b B_x)^2}{D + E_x},
\tag{3}
$$

$$
E_x' = E_x + \frac{1}{2}\frac{(g\mu_b B_x)^2}{D + E_x}.
\tag{4}
$$

The eigenstate of the Hamiltonian in Eq. (2) is described as $|0\rangle$, $|B\rangle = \frac{1}{\sqrt{2}}(|1\rangle + |-1\rangle)$, and $|D\rangle = \frac{1}{\sqrt{2}}(|1\rangle - |-1\rangle)$ where $|B\rangle$ and $|D\rangle$ are called a bright state and a dark state, respectively. We can control all the transitions between the ground state manifolds of NV centers by applying microwaves and RF fields as follows. The Hamiltonian of the NV center with external magnetic driving fields in our system is given by

$$
\begin{aligned}
H &= H_{NV} + H_{ex} \\
H_{ex} &= \sum_{j=x,y,z} \gamma_e B_{MW}^{(j)} \hat{S}_j \cos(\omega_{MW}t) + \gamma_e B_{RF}^{(j)} \hat{S}_j \cos(\omega_{RF}t),
\end{aligned}
\tag{5}
$$

where γ_e is the gyromagnetic ratio of the electron spin; B_{MW} and B_{RF} are the amplitudes of the microwave and RF fields, respectively; ω_{MW} and ω_{RF} are the driving frequencies of the MW and RF, respectively. To control the transition between $|0\rangle$ and $|B\rangle$ ($|D\rangle$), we can use microwave driving, as demonstrated in Ref. 18. In a rotating frame with $U = -\omega_{MW}|0\rangle\langle 0|$, the effective Hamiltonian is

$$
\begin{aligned}
H \simeq\ & (D - \omega_{MW} + E_x')|B\rangle\langle B| \\
& + (D - \omega_{MW} - E_x')|D\rangle\langle D| \\
& + \tfrac{1}{2}\gamma_e B_{MW}^{(x)}(|B\rangle\langle 0| + |0\rangle\langle B|) \\
& + i\tfrac{1}{2}\gamma_e B_{MW}^{(y)}(|D\rangle\langle 0| + |0\rangle\langle D|).
\end{aligned}
\tag{6}
$$

where we assume that $B_{MW} \neq 0$ and $B_{RF} = 0$; thus, we can induce Rabi oscillations between $|0\rangle$ and $|B\rangle$ ($|D\rangle$) using resonant microwave pulses with $\omega_{MW} = D + E_x'$ ($\omega_{MW} = D - E_x'$).

Moreover, we can control the transition between $|B\rangle$ and $|D\rangle$ using RF pulses. In a rotating frame with $U = \frac{1}{2}\omega_{RF}|B\rangle\langle B| - \frac{1}{2}\omega_{RF}|D\rangle\langle D|$, the effective Hamiltonian is

$$
\begin{aligned}
H \simeq\ & \left(D - \omega_{MW} + E_x' - \frac{1}{2}\omega_{RF}\right)|B\rangle\langle B| \\
& + \left(D - \omega_{MW} - E_x' + \frac{1}{2}\omega_{RF}\right)|D\rangle\langle D| \\
& + \frac{1}{2}\gamma_e B_{RF}^{(z)}(|B\rangle\langle D| + |D\rangle\langle B|),
\end{aligned}
\tag{7}
$$

where we assume that $B_{MW} = 0$ and $B_{RF} \neq 0$; thus, we can induce the coherent oscillation between $|B\rangle$ and $|D\rangle$ with $\omega_{RF} = 2E_x'$. To our best knowledge, such an experiment to induce the Rabi oscillation between $|B\rangle$ and $|D\rangle$ was not reported before.

We experimentally demonstrate the control of all transitions between ground state manifolds of the NV centers by magnetic driving fields at room temperature. Our experiment is performed with the same setup and sample as those in Ref. 34. Importantly, although an ensemble of NV centers is used in our experiment, we can, in principle, perform the same experiment using a single NV center. First, we measured the optically detected magnetic resonance (ODMR) spectra under simultaneously applied continuous-wave MW and RF fields, as illustrated in Fig. 2. In the case without RF fields, two dips are observed in Fig. 2 by sweeping the frequency of MW fields, which correspond to the transitions from $|0\rangle$ to $|B\rangle$ or $|D\rangle$. As a result, the resonance frequency between $|0\rangle$ and $|B\rangle(|D\rangle)$ is estimated to be 2.8768 GHz (2.8847 GHz). From these values, we determined the resonance frequency between $|B\rangle$ and $|D\rangle$, which was estimated to be approximately 7.9 MHz. Furthermore, we measured the CW-ODMR spectrum by applying the RF field with an approximate frequency of 7.9 MHz. As illustrated in Fig. 2, we detected four dips—a clear evidence of the coherent coupling between the RF fields and
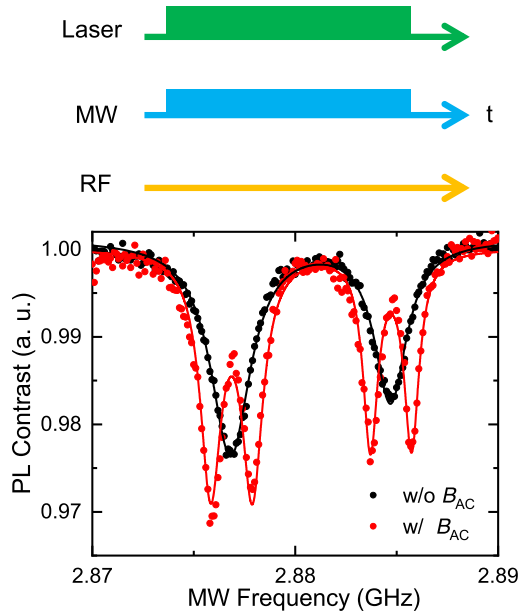
Fig. 2. (Color online) Pulse sequence of CW-ODMR without RF fields and CW-ODMR spectrum with and without RF fields under a magnetic field orthogonal to an NV axis.

the transition between $|B\rangle$ and $|D\rangle$. The splitting of each dip corresponds to the AT splitting induced by the RF fields. Secondly, we demonstrated Rabi oscillations between $|0\rangle$ and $|D\rangle$ ($|B\rangle$) by applying pulse MW fields. As illustrated in Fig. 3, clear Rabi oscillations can be observed by sweeping the pulse duration of MW fields with a resonant frequency between $|0\rangle$ and $|D\rangle$ ($|B\rangle$). The results confirm the π rotation between $|0\rangle$ and $|B\rangle$ ($|D\rangle$) with a pulse duration of about 210 ns.

Thirdly, we demonstrated the Rabi oscillations between $|B\rangle$ and $|D\rangle$. The pulse sequence is presented in Fig. 4(a). It is worth mentioning that the photoluminescence from the state of $|D\rangle$ is the same as that from the state of $|B\rangle$. Thus, to read
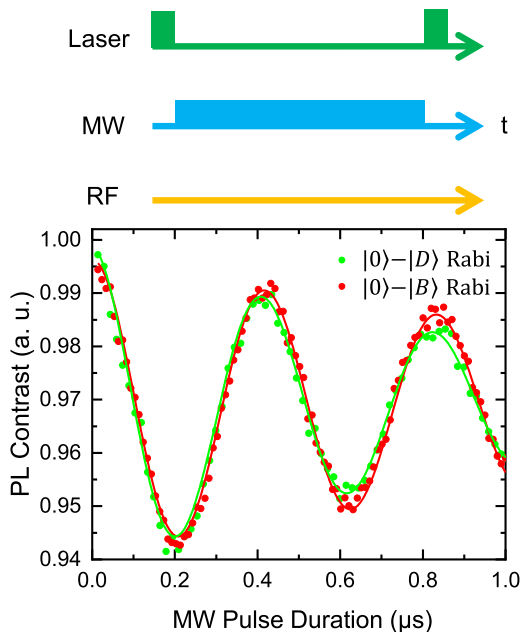

Fig. 3. (Color online) Pulse sequences and Rabi oscillations between $|0\rangle$ and $|B\rangle$($|D\rangle$)) by applying resonant MW fields. The green plots correspond to the Rabi oscillations between $|0\rangle$ and $|D\rangle$. The red plots correspond to the Rabi oscillations between $|0\rangle$ and $|B\rangle$.

out the state of $|B\rangle$, we shall convert the population of $|B\rangle$ into $|0\rangle$ by applying an MW π pulse and then read out the state of $|0\rangle$. The sequence of Rabi oscillations between $|B\rangle$ and $|D\rangle$ is as follows. First, we initialize the NV centers by a green laser, and the state is prepared in $|0\rangle$. Second, we apply the π pulse to completely transition from $|0\rangle$ to $|B\rangle$. Third, we implement the RF pulse, where its duration is swept. Finally, we read-out the state of $|B\rangle$ by applying the MW π and laser pulses. These experimental results are presented in Fig. 4(b). A clear oscillation can be observed, which confirms the coherent transition between the $|B\rangle$ and $|D\rangle$ states by applying an external magnetic field by the RF pulse. Therefore, we observed all the transitions between the ground state manifolds by applying an external AC magnetic field under a DC magnetic field orthogonal to the NV axis. Furthermore, we measured the $|B\rangle$–$|D\rangle$ Rabi oscillations for different frequencies and intensities of the applied RF pulses, as presented in Fig. 4(c). In the theory, the population difference, w, between $|B\rangle$ and $|D\rangle$ is given by

$$w(t; \Delta)$$
$$= -1 + \frac{2(\gamma_e B_{AC}^{(z)})^2}{(\gamma_e B_{AC}^{(z)})^2 + \Delta^2} \sin^2 \sqrt{(\gamma_e B_{AC}^{(z)})^2 + \Delta^2} \frac{t}{2}, \quad (8)$$

where $\Delta(=\omega_{RF} - 2E'_x)$ is the detuning from the resonance frequency. This analytical result as shown in Fig. 4(c) is consistent with the experimental result.

Finally, we investigated the coherence time of all transitions between the ground state manifolds of the NV centers by spin-echo with magnetic driving fields at room temperature. Especially, when we measure the coherence time between $|B\rangle$ and $|D\rangle$ states, we perform a π pulse with the resonant RF fields as illustrated in Fig. 5, and this is our unique approach. On the other hand, we measure the coherence time between $|0\rangle$ and $|B\rangle$($|D\rangle$)) by using a conventional way with microwave fields. For the spin-echo measurements, the first microwave pulse is a $\frac{\pi}{2}$ rotation while the final microwave pulse is also a $\frac{\pi}{2}$ rotation. However, in this case, some technical noise could be added. To remove such noise, we also perform another spin-echo experiment for a reference where the first microwave pulse is a $\frac{3\pi}{2}$ rotation while the final microwave pulse is also a $\frac{\pi}{2}$ rotation. By subtracting the spin-echo signal of the reference from that of the main experiment, we can improve the signal to noise ratio. Our results show that the coherence time between $|B\rangle$ and $|D\rangle$ states is about half of the coherence time between $|0\rangle$ and $|B\rangle$($|D\rangle$). This can be quantitatively understood as follows. Randomized electric fields or strain variations induce unexpected changes in frequencies of the $|B\rangle$ and $|D\rangle$, and this can be the main cause of decoherence.[18,48–50] The frequency shift between $|B\rangle$ and $|D\rangle$ due to the electric fields or strain is twice as large as that between $|B\rangle$ ($|D\rangle$)) and $|0\rangle$. This could explain the reason why the coherence time between $|B\rangle$ and $|D\rangle$ is shorter than that between $|B\rangle$ ($|D\rangle$)) and $|0\rangle$. To our best knowledge, this is the first experimental demonstration to measure the coherence time between the bright state and dark state of the NV centers with the resonant RF fields. Also, it is worth mentioning that such measurements of the coherence time with spin-echo is a significant difference from our previous results that perform only CW-ODMR.[34]
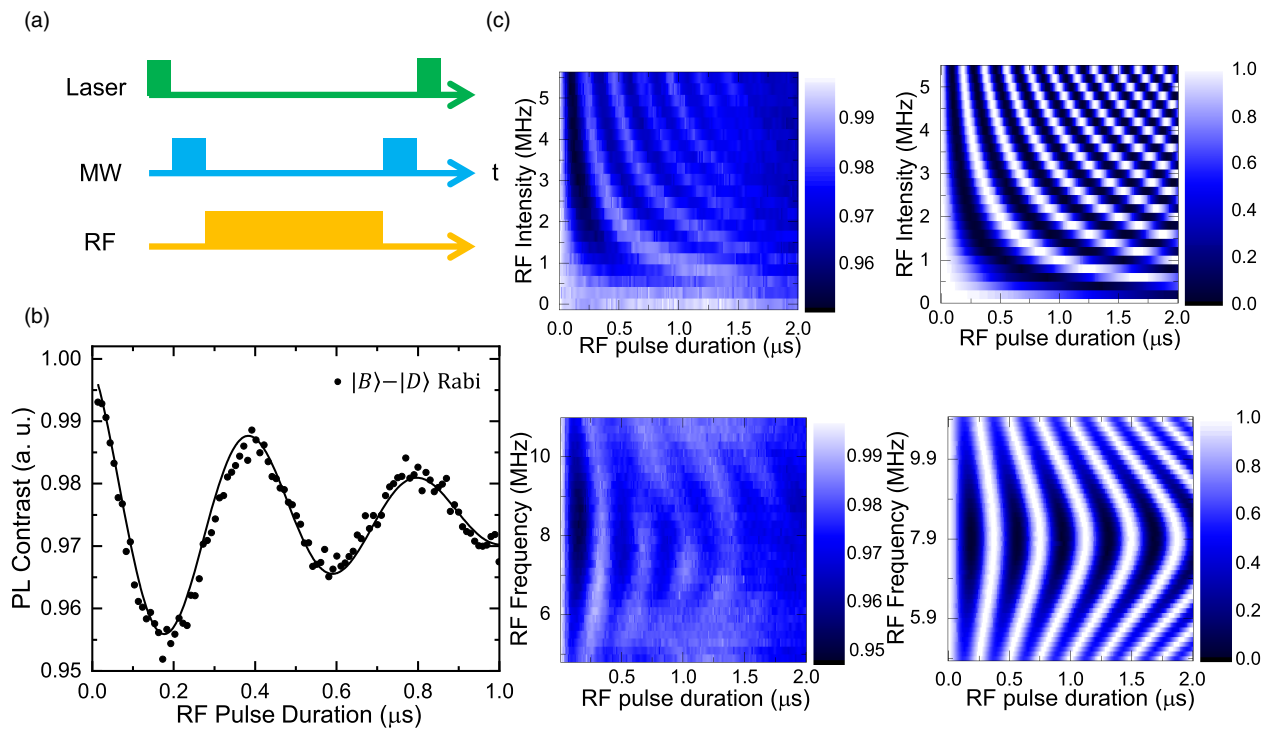
Fig. 4. (Color online) Rabi oscillation between $|B\rangle$ and $|D\rangle$ by resonant RF fields. (a) Sequence (b) experimental Rabi oscillation. Rabi oscillations between $|B\rangle$ and $|D\rangle$ by resonant RF fields for various (c) intensities and frequencies of RF fields. The figures on the left and right present the experimental results and theoretical calculations, respectively.
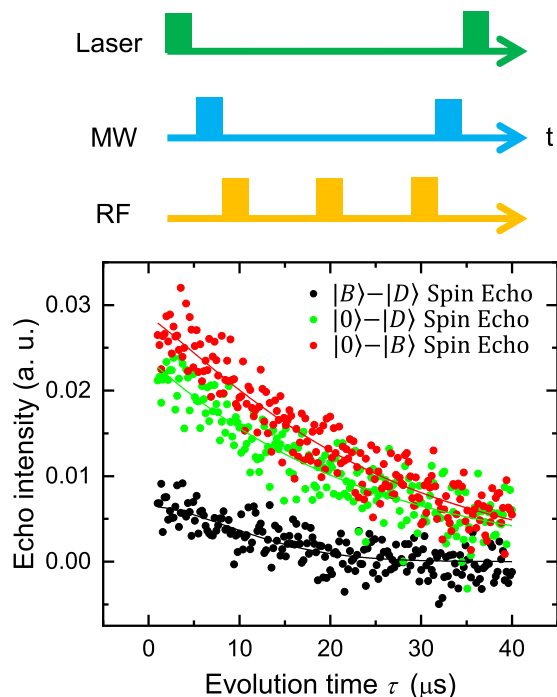
Fig. 5. (Color online) Pulse sequence of spin-echo between $|B\rangle$ and $|D\rangle$ where we perform a π pulse by resonant RF fields between $|B\rangle$ and $|D\rangle$. Also, we show the results of spin-echo between ground state manifolds of the NV centers. It is worth mentioning that we measure the spin-echo between $|B\rangle(|D\rangle)$ and $|0\rangle$ by a conventional way with resonant microwave fields.

In conclusion, we demonstrated the control of the three transitions among the ground state sublevels of the NV centers by applying external magnetic driving fields and observing the Rabi oscillations between all the transitions.

Especially, the unique point of our approach is to utilize RF fields to induce the Rabi oscillations between a bright state and dark state of the NV centers. Moreover, we measure the coherence time between ground state manifolds of the NV centers by spin-echo techniques where we perform a π pulse between the bright state and dark state with the resonant RF fields. Our technique is significantly simpler than those of previous reports where the mechanical vibration is required to perform quantum manipulation of all the transitions. Owing to the simplicity of our scheme, our results pave the way for the exploitation of the full potential of a spin 1 system.

ORCID iDs   Yuichiro Matsuzaki https://orcid.org/0000-0001-6814-3778   Norikazu Mizuochi https://orcid.org/0000-0003-3099-3210   Junko Ishi-Hayase https://orcid.org/0000-0002-4238-305X

1) M. V. G. Dutt, Science **316**, 1312 (2007).
2) T. H. Taminiau, J. Cramer, T. Van Der Sar, V. V. Dobrovitski, and R. Hanson, Nat. Nanotechnol. **9**, 171 (2014).
3) G. Balasubramanian et al., Nat. Mater. **8**, 383 (2009).
4) N. Mizuochi et al., Phys. Rev. B **80**, 041201 (2009).
5) E. D. Herbschleb et al., Nat. Commun. **10**, 3766 (2019).
6) H. Bernien et al., Nature **497**, 86 (2013).
7) P. C. Humphreys, N. Kalb, P. Jaco, J. Morits, R. N. Schouten, R. F. L. Vermeulen, D. J. Twitchen, M. Markham, and R. Hanson, Nature **558**, 268 (2018).
8) S. Yang et al., Nat. Photonics **10**, 507 (2016).
9) K. Tsurumoto, R. Kuroiwa, H. Kano, Y. Sekiguchi, and H. Kosaka, Commun. Phys. **2**, 74 (2019).
10) W. Pfaff et al., Science **345**, 532 (2014).

11) N. Y. Yao, L. Jiang, A. V. Gorshkov, P. C. Maurer, G. Giedke, J. I. Cirac, and M. D. Lukin, Nat. Commun. **3**, 800 (2012).
12) M. W. Doherty, N. B. Manson, P. Delaney, F. Jelezko, J. Wrachtrup, and L. C. Hollenberg, Phys. Rep. **528**, 1 (2013).
13) J. M. Taylor, P. Cappellaro, L. Childress, L. Jiang, D. Budker, P. R. Hemmer, A. Yacoby, R. Walsworth, and M. D. Lukin, Nat. Phys. **4**, 810 (2008).
14) L. Rondin, J. P. Tetienne, T. Hingant, J. F. Roch, P. Maletinsky, and V. Jacques, Rep. Prog. Phys. **77**, 056503 (2014).
15) T. Wolf, P. Neumann, K. Nakamura, H. Sumiya, T. Ohshima, J. Isoya, and J. Wrachtrup, Phys. Rev. X **5**, 041001 (2015).
16) D. Le Sage, K. Arai, D. R. Glenn, S. J. Devience, L. M. Pham, L. Rahn-Lee, M. D. Lukin, A. Yacoby, A. Komeili, and R. L. Walsworth, Nature **496**, 486 (2013).
17) E. V. A. N. Oort and M. Glasbeek, Chem. Phys. Lett. **168**, 529 (1990).
18) F. Dolde et al., Nat. Phys. **7**, 459 (2011).
19) F. Dolde et al., Phys. Rev. Lett. **112**, 097603 (2014).
20) E. H. Chen, H. A. Clevenson, K. A. Johnson, L. M. Pham, D. R. Englund, P. R. Hemmer, and D. A. Braje, Phys. Rev. A **95**, 053417 (2017).
21) T. Mittiga et al., Phys. Rev. Lett. **121**, 246402 (2018).
22) J. Michl et al., Nano Lett. **19**, 4904 (2019).
23) V. M. Acosta, E. Bauch, M. P. Ledbetter, A. Waxman, L. S. Bouchard, and D. Budker, Phys. Rev. Lett. **104**, 070801 (2010).
24) P. Neumann et al., Nano Lett. **13**, 2738 (2013).
25) G. Kucsko, P. C. Maurer, N. Y. Yao, M. Kubo, H. J. Noh, P. K. Lo, H. Park, and M. D. Lukin, Nature **500**, 34 (2013).
26) H. Clevenson, M. E. Trusheim, C. Teale, T. Schröder, D. Braje, and D. Englund, Nat. Phys. **11**, 393 (2015).
27) D. M. Toyli, C. F. de las Casas, D. J. Christle, V. V. Dobrovitski, and D. D. Awschalom, Proc. Natl Acad. Sci. **110**, 8417 (2013).
28) T. Plakhotnik, M. W. Doherty, J. H. Cole, R. Chapman, and N. B. Manson, Nano Lett. **14**, 4989 (2014).
29) N. Wang et al., Phys. Rev. X **8**, 11042 (2018).
30) Y. Matsuzaki, H. Morishita, T. Shimooka, T. Tashima, K. Kakuyanagi, K. Semba, W. J. Munro, H. Yamaguchi, N. Mizuochi, and S. Saito, J. Phys.: Condens. Matter **28**, 275302 (2016).
31) K. Hayashi et al., Phys. Rev. Appl. **10**, 034009 (2018).
32) K. Fang, V. M. Acosta, C. Santori, Z. Huang, K. M. Itoh, H. Watanabe, S. Shikata, and R. G. Beausoleil, Phys. Rev. Lett. **110**, 130802 (2013).
33) S. Saijo, Y. Matsuzaki, S. Saito, T. Yamaguchi, I. Hanano, H. Watanabe, N. Mizuochi, and J. Ishi-Hayase, Appl. Phys. Lett. **113**, 082405 (2018).
34) T. Yamaguchi, Y. Matsuzaki, S. Saito, S. Saijo, H. Watanabe, N. Mizuochi, and J. Ishi-Hayase, Jpn. J. Appl. Phys. **58**, 100901 (2019).
35) X. Zhu, Y. Matsuzaki, R. Amsüss, K. Kakuyanagi, T. Shimo-Oka, N. Mizuochi, K. Nemoto, K. Semba, W. J. Munro, and S. Saito, Nat. Commun. **5**, 3524 (2014).
36) Y. Matsuzaki et al., Phys. Rev. Lett. **114**, 120501 (2015).
37) Y. Kubo et al., Phys. Rev. Lett. **105**, 140502 (2010).
38) A. Vepsäläinen, S. Danilin, and G. Sorin Paraoanu, Sci. Adv. **5**, eaau5999 (2019).
39) A. Barfuss et al., Nat. Phys. **14**, 1087 (2018).
40) F. Jelezko, T. Gaebel, I. Popa, A. Gruber, and J. Wrachtrup, Phys. Rev. Lett. **92**, 076401 (2004).
41) C. G. Yale, B. B. Buckley, D. J. Christle, G. Burkard, F. J. Heremans, L. C. Bassett, and D. D. Awschalom, Proc. Natl Acad. Sci. **110**, 7595 (2013).
42) D. A. Golter and H. Wang, Phys. Rev. Lett. **112**, 116403 (2014).
43) E. R. Macquarrie, T. A. Gosavi, N. R. Jungwirth, S. A. Bhave, and G. D. Fuchs, Phys. Rev. Lett. **111**, 227602 (2013).
44) E. R. MacQuarrie, T. A. Gosavi, A. M. Moehle, N. R. Jungwirth, S. A. Bhave, and G. D. Fuchs, Optica **2**, 233 (2015).
45) H. Y. Chen, S. A. Bhave, and G. D. Fuchs, Phys. Rev. Applied **13**, 054068 (2020).
46) P. V. Klimov, A. L. Falk, B. B. Buckley, and D. D. Awschalom, Phys. Rev. Lett. **112**, 087601 (2014).
47) A. Barfuss, J. Teissier, E. Neu, A. Nunnenkamp, and P. Maletinsky, Nat. Phys. **11**, 820 (2015).
48) Y. Matsuzaki et al., Phys. Rev. A **91**, 042329 (2015).
49) P. Jamonneau et al., Phys. Rev. B **93**, 024305 (2016).
50) S. Kobayashi, Y. Matsuzaki, H. Morishita, S. Miwa, Y. Suzuki, M. Fujiwara, and N. Mizuochi, Phys. Rev. Applied **14**, 044033 (2020).